Dynamic X-ray diffraction observation of shocked solid iron up to 170 GPa

A. Denoeud[a], N. Osaki[b,c], A. Benuzzi-Mounaix[a,d], H. Uranishi[b], Y. Kondo[b], R. Kodama[b,c], E. Brambrink[a], A. Ravasio[a], M. Bocoum[a], J.-M. Boudenne[a], M. Harmand[e], F. Guyot[e], S. Mazevet[d], D. Riley[f], M. Makita[f], T. Sano[g], Y. Sakawa[g], Y. Inubushi[h], G. Gregori[i], M. Koenig[a,j] and G. Morard[e]

[a] *Laboratoire pour l'Utilisation des Lasers Intenses (LULI), Ecole Polytechnique, CNRS, CEA, UPMC, 91128 Palaiseau, France* [b] *Graduate School of Engineering, Osaka University, 2-1 Yamada-oka, Suita, Osaka 5650871, Japan* [c] *Photon Pioneers Center, Osaka University, 2-1 Yamada-oka, Suita, Osaka 5650871, Japan* [d] *LUTH, Observatoire de Paris, CNRS, Université Paris Diderot, 92195 Meudon, France* [e] *Institut de Minéralogie, de Physique des Matériaux et Cosmochimie (IMPMC), MNHN, CNRS, UPMC, IRD, Sorbonne Universités, 75005 Paris, France* [f] *Queens Univ Belfast, Sch Math & Phys, Ctr Plasma Phys, Univ Rd, Belfast BT7 1NN, Antrim, North Ireland* [g] *Institute of Laser Engineering, Osaka University, 2-6 Yamada-oka, Suita, Osaka 5650871, Japan* [h] *RiKEN Spring-8 Center,Sayo, Hyogo 679-5148, Japan* [i] *Department of Physics, University of Oxford, OX1 3PU, United Kingdom* [j] *Institute for Academic Initiatives, Osaka University, Suita, Osaka 565-0871, Japan*

Submitted to Proceedings of the National Academy of Sciences of the United States of America

Investigation of the iron phase diagram under high pressure and temperature is crucial for the determination of the compositions of the cores of rocky planets and for better understanding the generation of planetary magnetic field. Here we present X-ray diffraction results from laser-driven shock-compressed single-crystal and polycrystalline iron indicating the presence of solid hcp iron up to pressure at least 170 GPa along the principal Hugoniot, corresponding to a temperature of 4,150 K. This is confirmed by the agreement between the pressure obtained from the measurement of the iron volume in the sample and the inferred shock strength from velocimetry (VISAR) measurements. Our results, obtained by fast shock compression of the iron sample, also agree with recent experiments where the iron is statically compressed using a diamond anvil cells (melting of hcp structure occurs at 4,600 K for 170 GPa). Thus, while static compression methods are limited in the achievable pressures and temperatures, our dynamic compression method do not present such limitation and it can be applied to study conditions that are relevant to Earth and super-Earths cores.

X-ray diffraction | iron phase diagram | shock-compressed iron | earth core | dynamic compression

Iron is the main constituent of Earth and telluric planetary cores. Therefore, due to this geophysical interest, its phase diagram under high pressure and temperature has been extensively studied by static[1-3] or dynamic[4-8] compression techniques. In particular, the determination of its melting curve at the Earth's Inner-Outer Core Boundary constrains the thermodynamics that governs the Earth's heat budget and dynamics such as the heat flux from the core to the mantle, the power available for the geodynamo and the planetary cooling rate[9]. Besides, the knowledge of the exact crystalline structure of iron at appropriate pressure and temperature is a key parameter to explain seismological observations. In fact, having an hexagonal close packed (hcp) structure under Earth's inner core conditions (360 GPa and ∼6000 K) is mandatory to explain its anisotropic structure observed by seismology[10,11].

Iron and its alloys have been widely studied by static compression in associating large volume cells or diamond anvils cells (DAC) with a probing synchrotron radiation source[12,13]. In addition to the study of the solid-solid phase transitions, like body centered cubic (bcc)- face centered cubic (fcc) in temperature and bcc-hcp in pressure, and to the measurement of some properties of these phases[14-16], X-ray diffraction also allows to study the solid-liquid transitions[17] and to measure the liquid density[18]. Recently, the static melting curve of pure iron has been measured up to 150 GPa thanks to this technique[2]. However, static compression methods are limited in pressure and in temperature and do not allow to reach with precision the high P-T conditions that are relevant to Earth and super-Earths core, i.e. over 300 GPa and 5000 K. Indeed, to reach such conditions with static compression techniques, it becomes necessary to decrease the size of the sample. This involves various problems of gradient and inhomogeneity through the studied material as well as chemical reaction and thermal diffusion with the diamonds, which limits nowadays the reachable temperature at around 5000 K[16].

It thus becomes necessary to perform dynamic compression to reach higher temperature/pressure conditions of relevance for planetology. This can be done with high power lasers by using shock or quasi-isentropic compression techniques[19-20]. However, discrepancies observed between shock and static studies of iron over 100 GPa have been attributed to non-equilibrium processes[21], invalidating the possibility to properly probe phase diagrams of geophysically relevant materials using dynamic compression. Different features, such as overheating or presence of a new crystalline structure in iron just below the melting curve, have been described in shock experiments in contradiction with static experiments. Here we aim at addressing these controversies by probing shock-compressed iron at the nanosecond and picosec-

Significance

Iron is the main constituent of the core of rocky planets; therefore understanding its phase diagram under extreme conditions is fundamental to model their evolution. Using dynamic compression by laser driven shocks, pressure and temperature conditions close to what is found in these cores can be reached. However, it remains unclear whether phase boundaries determined at nanosecond time-scale agree with static compression performed using diamond anvil cell. Here we observed the presence of solid hcp iron at 170 GPa and 4,150 K, consistent with recent static compression data. This X-ray diffraction experiment is therefore the first direct proof that dynamic laser compression is suitable for studying iron at conditions of deep planetary interiors difficult to achieve with static compression techniques.

Reserved for Publication Footnotes

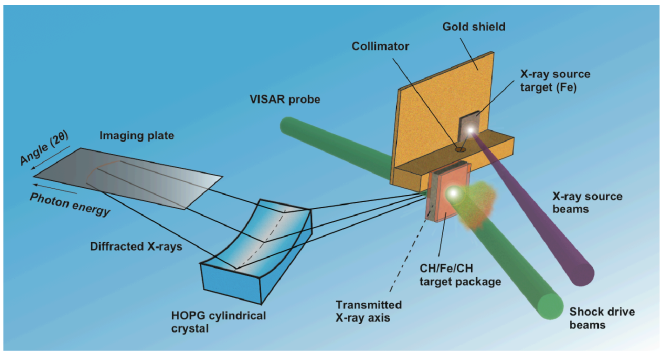

Fig. 1. Experimental pump-probe set up and targets configuration at GEKKO XII. The angular-resolved spectrometer was made by a defocused cylindrical Von Hamos geometry. For a better understanding of the geometry, the shielding of the spectrometer that surrounds the HOPG crystal and the Image Plate is not represented here.

ond time-scales using X-ray diffraction (XRD), thus providing a direct measurement of its structure.

Structural XRD studies of iron at nanosecond or better time resolution[22-24], have been, so far, focused on the low-pressure bcc-hcp transition and on measuring the c/a ratio of the hcp phase at low pressure. Consequently, those experiments did not collect diffracted signal from iron compressed at more than few tens of GPa. At higher pressures, because of both the higher velocity of the shock and the quicker release of the shock-compressed iron, the time duration of the X-ray probe must be short enough to avoid integrating inhomogeneous hydrodynamic conditions. Moreover, at these more extreme conditions, the incoherent scattering from the laser-ablated plasma cannot always be neglected as it can disturb the collected signal.

To overcome these issues, we have collected diffracted signals from shock-compressed iron using a large analyzer crystal (which increases the signal-to-noise ratio and allows the separation between coherent and incoherent scattering) and an X-ray source produced by either a picosecond or a nanosecond laser. Even if this technique cannot collect the signal over a large range of angles, the advantage of separating the different spectral components can significantly reduce the uncertainties in identifying the elastic signal contribution and thus increase accuracy in structure determination.

Two diffraction experiments were performed using different time durations for the X-ray probe. The nanosecond resolution XRD experiment was performed on the GEKKO XII laser facility at the Institute of Laser Engineering at the Osaka University and the picosecond one on the LULI 2000 / PICO 2000 laser facility at the Laboratoire pour l'Utilisation des Lasers Intenses at the Ecole Polytechnique. This second experiment and its results, which support the findings and conclusions of the first one, are presented in the supplementary material. The experimental scheme of the nanosecond experiment is shown in Fig.1, and description of the experimental procedure is presented in the Methods section.

Three diffractograms obtained with an angle-resolved Von Hamos spectrometer and a nanosecond resolution on different laser shots are presented in Fig. 2.a). As shown, the use of the crystal introduces spherical aberrations, as the radiation were angularly scattered on a curve. These aberrations were corrected in our analysis by ray tracing and the corresponding diffraction patterns are presented on the right of the same figure.

Diffraction signal from undriven (i.e. without compressing the sample) polycrystalline iron comes only from the bcc phase of iron (blue line in Fig. 2.b)), the iron phase stable at ambient pressure and temperature conditions. This shot indicates that our diffractometer system was able to collect diffracted signal from polycrystalline iron with a good signal to noise ratio. The width of the diffraction peak (3.1° full width at half maximum) is in good agreement with the angular resolution of the diffractometer (3°). This demonstrates that the chosen scattering geometry and shielding are sufficient to remove any spurious signal coming directly from the X-ray source. Finally, this provides a refined angular calibration of the spectrometer, as the maximum of the diffracted signal comes from the (011) planes of the bcc phase of iron at 6.7 keV (corresponding to 54.4°).

Diffraction patterns were then collected on iron samples shock-compressed using a drive laser, whose intensity was high enough to induce a transition to the hcp phase in iron. Shots performed with a laser energy close to 180 J at 532 nm and with a higher one, close to 300 J at 532 nm, are also shown in Fig. 2. A VISAR system (see methods) allowed us to determine the pressure induced by the shock in iron to be 100 +/- 10 GPa in the first case and 170 +/- 17 GPa in the second case. New diffraction maxima appear which are consistent with the (101) most intense diffraction peaks of hcp iron. Moreover, we notice that the (011) diffraction line of bcc iron remains visible at 54°. We note that these diffraction results were also observed with a picosecond resolution up to 184 +/- 24 GPa on the LULI2000 laser facility, as explained and illustrated in the supplementary material.

To understand the diffraction data, we have performed radiation-hydrodynamic simulations of the laser-induced shock propagation in iron (Fig. 3). In the GEKKO configuration, the X-ray spectrometer collects the diffracted signal from iron from the rear surface (i.e., opposite to the laser illumination). In this geometry, adjustment of the iron thickness and of the pump-probe delay allowed us to control accurately the P-T conditions despite the low temporal resolution. The diffracted X-rays collected by the analyzer crystal came mostly from the first rear side microns of iron due to strong X-ray absorption in iron (Fig. 3, on bottom). Indeed, 50% of the X-rays are already absorbed in the first 7 µm of iron. Consequently, most of the diffracted signal collected by the spectrometer comes from uncompressed cold iron (see blue box in Fig. 3), which explains the persistence of the $(011)_{bcc}$ peak of cold iron even in the case of shock-compressed samples (Fig. 2). We have thus calculated the diffracted signal coming from various depths in iron over the entire duration of the X-ray probing. In this way, the decrease in intensity of this $(011)_{bcc}$ peak indicates that iron is partially transforming into the hcp phase as it gets shocked. Moreover, at 170 GPa, the $(011)_{bcc}$ intensity decreases even further. The decrease of the scattered peak intensity could also be explained by pre-heating of the cold iron due to an increase of the Debye Waller factor. Here we don't observe signature of pre-heating as the diffraction peak of the fcc phase of iron is not observed. In addition the simulations described below are supported this observation. Therefore the decay of the $(011)_{bcc}$ peak intensity can be easily explained by the increase of the shock velocity, which induces a decrease of the volume of iron that remained uncompressed. Furthermore, it can be noticed that this configuration allowed us to probe relatively homogeneous hydrodynamic conditions over a 1.6 ns duration and a 20 µm iron thickness. The estimated inhomogeneity in pressure from the simulation was then lower than 10% for the highest laser intensities reached here, as shown below.

Diffraction peaks of the hcp phase of iron are expected in the angular range 48°-72°, near 6.7 keV, corresponding to $(100)_{hcp}$, $(002)_{hcp}$ and $(101)_{hcp}$. Theoretical positions of these peaks calculated for the pressures measured by the VISAR system and for an hcp c/a ratio of 1.61 are given in Fig. 2 (dashed lines). Their predicted heights have been normalized to the intensity of the experimental signal. The first diffraction peak corresponding to $(100)_{hcp}$, is too close to the $(011)_{bcc}$ to be detectable, due to the limited angular resolution. Nevertheless, a shoulder can be observed on $(011)_{bcc}$ for the highest pressure (red line) at 57°,

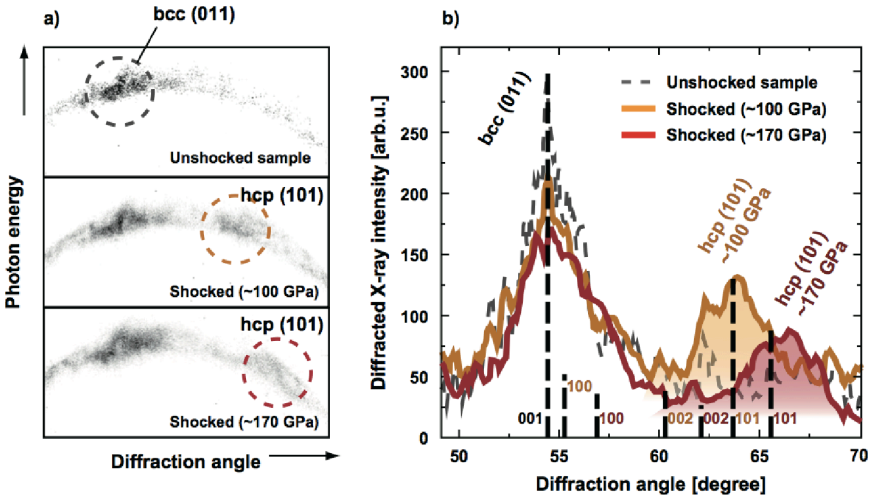

Fig. 2. On the left: raw diffractograms collected in reflection by the defocused Von Hamos spectrometer on three different laser shots. The first order used for the crystal configuration introduced spherical aberrations, corrected in our analysis. On the right: angular profiles of the diffracted signal after this correction (color lines) and theoretical predictions at the pressure measured by the VISAR system (black dashed lines normalized in height at the experimental signal).

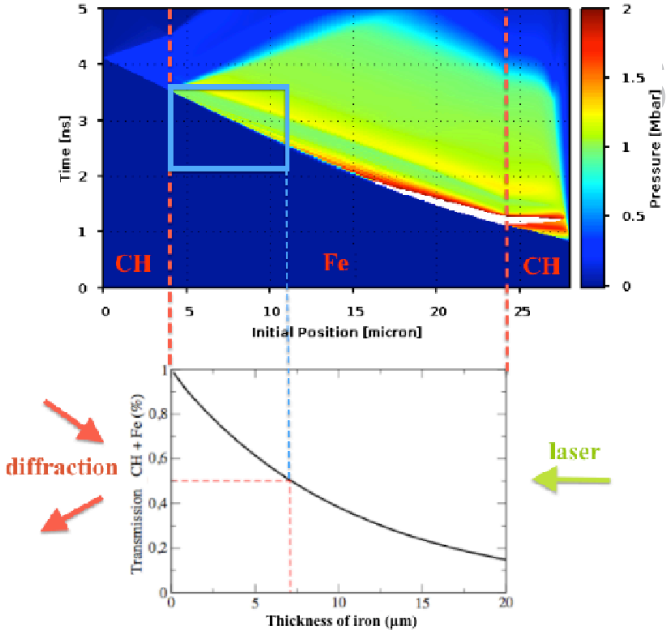

Fig. 3. On top: hydrodynamic simulation made with the pulse features of the GEKKO XII laser and an intensity of 5.10^{12} W/cm^2. The probe was sent 1.1 ns later than the pump laser generating the shock (here at 1.0 ns). The rectangular box in blue defines the spatial and temporal windows probed by the X-rays, taking into account the absorption on a round trip in CH and iron (bottom graph). The analysis took in consideration the whole thickness of the target. In this layout, a large part of the probed iron was still at ambient pressure and temperature. Integrating spatially and temporally the hydrodynamic conditions of the probed shocked iron gave an average pressure of 106 +/- 7 GPa. The uncertainty corresponds to the standard deviation of the reached pressures in the 20 µm 1.6 ns temporal and spatial windows investigated.

when this peak is moved further away from the bcc peak at 54.4°. The $(002)_{hcp}$ peak could not be detected in shock-compressed samples. This could be related to its low intensity, due to potential alignment with the compression axis, as already observed in DAC experiments[25]. Conversely, the $(101)_{hcp}$ peak was clearly detected on the two spectra of shock-compressed iron (see Fig. 2) and allowed us to identify the phase transition of iron to the hcp structure. Indeed, it should be noticed that neither diffraction peaks from the bcc phase nor ones from the fcc phase could occur at such a diffraction angle at such conditions of pressure and density. Moreover, the (101) reflection of the possible dhcp phase should be well visible at ~57.4° and ~59.2°, respectively at around 100 GPa and 170 GPa. This is clearly not the case in our data. The c/a ratio of hcp iron could not be directly measured due to the lack of additional peaks. We inferred this ratio to be 1.61, following the results of recent LH-DAC experiments (giving c/a ~1.61 at pressures of around 160 GPa and temperatures between 2000 K and 4000 K)[16]. In fact, uncertainties due to variations of this ratio between 1.59 and 1.62 would be lower than the experimental uncertainties on the peak positions. Moreover, such a ratio is also mentioned in previous dynamic compression studies[24]. Using the diffraction angle measurement and the inferred hcp c/a ratio of 1.61[16,23], the position of the $(101)_{hcp}$ diffraction peak allowed us to estimate the iron compression factor.

The consistency of our data is reinforced by the agreement between pressure deduced by VISAR measurements and pressure deduced from diffraction peaks of hcp structure. The theoretical volume of a unit cell of the hcp phase of iron at 100 +/- 10 GPa and 10.87 +/- 0.15 g/cm^3 (density deduced from the Hugoniot curve[8]) is 17.05 +/- 0.25 Å^3. The corresponding $(101)_{hcp}$ diffraction peak would then be located at 63.7 +/- 0.4°. This result is in very good agreement with the measured angular position at 63.7° +/- 0.2°. At 170 +/- 17 GPa and 11.78 +/- 0.17 g/cm^3, the corresponding volume of the unit cell is 15.74 +/- 0.23 Å^3 giving a $(101)_{hcp}$ diffraction peak at 65.6 +/- 0.4°. In this case, the predicted position of the diffraction peak is slightly different from the measured one, located at 66.3 +/- 0.2°, corresponding to an iron density of 12.07 +/- 0.09 g/cm^3 and thus a pressure of 198 +/- 8 GPa. This small discrepancy might be explained by larger pressure gradients across the sample during the probing time or by differences with the c/a ratio used. Indeed, from hydrodynamic simulation made at the experimental laser intensity of $8.5x10^{12}$ W/cm^3 we infer a time and spatial integrated pressure of 173 +/- 16 GPa.

Using both an angular and energy resolved spectrometer, we have thus measured a diffracted signal from highly shock-compressed iron. Our observations indicate the presence of an hcp structure in the iron phase diagram up to at least ~170 GPa on the Hugoniot. This is in good agreement with recent experiments in laser-heated diamond cell up to 330 GPa and 5000 K showing the occurrence of the hcp structure of iron over a wide P-T range[16], whereas other structures, such as bcc or dhcp, had been suggested under these P-T conditions[26-27]. This is also in very good agreement with the results of our picosecond X-ray

diffraction experiments made on single-crystal iron and shown in the supplementary material.

Methods

The backlighter and the main target were mounted on a 100 µm-thick gold support designed to shield the X-ray spectrometer from any direct view of the X-ray probe radiation. Two holes of 200 µm-diameter were cut through the gold shielding, between the two targets, and were used to determine the scattering geometry and the 3° angular aperture of the X-ray source. The backlighter target consisted of a 25 µm-thick iron foil. Nine long pulse-laser beams (2.5 ns pulse duration) that each delivered 125 J at 351 nm in a 100 µm-diameter focal spot, corresponding to a total intensity close to 10^{16} W / cm^2, illuminated this foil to create an X-ray source of He-α emission at 6.7 keV. This emission was monitored by a streak camera and a pinhole camera for each shot. The duration of the X-ray emission was measured to be 1.6 +/- 0.2 ns FWHM. The main sample target consisted in 20-µm polycrystalline iron, enclosed by 4 µm thick plastic coating. Up to three long-pulse laser beams (2.5 ns pulse duration) at 532 nm were focussed on this target to drive a shock wave in the iron and to bring the sample to high pressures. These beams were spatially smoothed with Kinoform Phase Plate (KPP) to achieve a flat top focal spot of 1 mm diameter. This is needed in order to have a uniform shock profile across the sample. The energy of each of these laser beams was set at ∼200 J at 532 nm. The total intensity in the focal spot was varied between 10^{12} and 10^{13} W / cm^2.

A VISAR system (Velocity Interferometer System for Any Reflector)[28] was used to control the planarity of the shock and the thermodynamical state of the sample at the probing time. From this optical system, we were able to measure the mean shock velocity in the thin rear layer of plastic using the shock transit time and the initial thickness. These measurements were coupled to hydrodynamic simulations (using the radiation hydrodynamic MULTI code[29]) to infer the thermodynamical conditions of the iron sample at the probed time and to extract pressure and temperature conditions. We used a new equation of state (EOS) table for iron[8] in these hydrodynamic simulations, that combines *ab initio* calculations with the last experimental phase transitions results[2] and the EOS SESAME 2150. It should be noticed that the transit time of the shock did not depend on the EOS used in the simulations. Moreover, this new EOS was also used to extract the experimental density and then to find the theoretical positions of the diffraction peaks from the different solid phases of iron, under certain assumptions on their mesh ratio, as previously explained.

We used a ZYA-quality cylindrical HOPG (*highly oriented pyrolytic graphite*) crystal (with mosaic spread 0.4 +/- 0.1°; plane separation 2d = 6.71 Å, and radius of curvature 110 mm) in a modified Von Hamos configuration. The HOPG properties[30] allowed us to maximize the crystal reflectivity and consequently the number of collected photons when the crystal is used in its mosaic-focusing mode. The axis of the cylinder was given by the source/detector direction. In the (symmetrical) classical Von Hamos geometry, the increase in the collection solid angle is achieved by focusing all of the collected angles on the same line that does not permit any spatial resolution. To obtain spatial resolution, we modified this geometry by defocusing the collected X-ray beam on the detector, as shown in Fig.1. This was achieved by reducing the source-crystal and crystal-detector distances from the ideal Von Hamos geometry, while keeping those distances equal in order to maintain the mosaic focusing mode of the HOPG. In this new geometry, the collected angles were then scattered on a perpendicular line from the crystal axis, whereas different energies were encoded on parallel rays. The HOPG crystal was operated in its first diffraction order. The diffraction order, the size of the crystal (100 x 50 mm^2) and the size of the image plate detector (IP) set the angular detection range at 24°. The crystal spectrometer was oriented such as its axis was aligned at 60 +/- 2° from the X-ray probe axis. This allowed to collect the diffracted signal from both the cold iron bcc structure and highly compressed hcp structure. Due to the large mosaicity of the crystal, the intrinsic angular resolution of this spectrometer was around 0.3°, which is again much lower than the angular aperture of the X-ray source. Finally, the whole system was placed in a shielding 2 mm-stainless steel box. Moreover, a 50 µm mylar sheet was placed on the entrance slit to protect the HOPG crystal and the image plates were surrounded by 13 µm of aluminum.

ACKNOWLEDGMENTS.

We acknowledge the expert support from the technical groups at LULI2000 and GEKKO XII facilities, in particular Philippe Vacar for his valuable help in the manufacture of the spectrometers. We also would like to thank Jacques Chevallier from the Department of Physics and Astronomy of the University of Aarhus (Denmark) for the synthesis of Fe single crystals targets. Moreover, the crystallographic data for the orientation of iron single crystals were collected at the X-ray diffraction platform of IMPMC and we thank Benoît Baptiste for his support. This work was supported by PlanetLab program of French National Research Agency (ANR) grant no. ANR-12-BS04-0015-04 and also supported partially by JSPS KAKENHI (Grant Numbers 22224012), JSPS core to core program on International Alliance for Material Science in Extreme States with High Power Laser and XFEL, and Xray Free Electron Laser Priority Strategy Program (MEXT).

1 R. Boehler, *Nature,* **363**, 534 (1993)
2 S. Anzellini *et al.*, *Science,* **340**, 464 (2013)
3 Q. Williams *et al.*, *Science,* **236**, 181 (1987)
4 C. S. Yoo *et al.*, *Phys. Rev. Lett.,* **70**, 3931 (1993)
5 J. H. Nguyen and N. C. Holmes, *Nature,* **427**, 339 (2004)
6 J. M. Brown and R. G. McQueen, *J. Geophys. Res.,* **91**, 7485 (1986)
7 G. Huser *et al.*, *Phys. of Plasmas,* **12**, 060701 (2005)
8 M. Harmand *et al.*, *arXiv:1411.2074* (2014)
9 T. Lay et al., *Nat. Geosci.,* **1**, 25 (2008)
10 A. Lincot *et al., Comptes Rendus Geoscience,* **346**, 148-157 (2014)
11 A. Deuss, *Annual Review of Earth and Planetary Sciences*, **42**, 103-126 (2014)
12 J. C. Jamieson and A. W. Lawson, *Journal of Applied Physics*, **33**, 776 (1962)
13 T. Takahashi and W. A. Bassett, *Science,* **145**, 483 (1964)
14 H. Mao *et al., Journal of Applied Physics*, **38**, 272 (1967)
15 W. A. Bassett and E. Huang, *Science,* **238**, 780 (1987)
16 S. Tateno *et al., Science,* **330**, 359 (2010)
17 G. Morard *et al.*, *Physics and Chemistry of Minerals,* **38**, 767 (2011)
18 G. Morard *et al.*, *High Pressure Research,* **34**, 9 (2014)
19 R. F. Smith *et al.*, *Nature,* **511**, 330 (2014)
20 N. Amadou *et al.*, *High Energy Density Physics,* **9**, 243 (2013)
21 S. N. Luo and T. J. Ahrens, *Phys. Earth Plan. Inter.*, **143-144**, 369-386 (2004)
22 D. H. Kalentar *et al.*, *Phys. Rev. Lett.,* **95**, 075502 (2005)
23 J. Hawreliak *et al.*, *Phys. Rev. B.,* **74**, 184107 (2006)
24 J. Hawreliak *et al.*, *Phys. Rev. B.,* **83**, 144114 (2011)
25 H. R. Wenk *et al.*, *Nature,* **405**, 1044 (2000)
26 L. Dubrovinsky *et al.*, *Science,* **316**, 1880 (2007)
27 D. Andrault *et al.*, *Science,* **276**, 831 (1997)
28 L. M. Barker and R. E. Hollenbach, *Journal of Applied Physics*, **43**, 4669 (1972)
29 R. Ramis *et al.*, *Computer Physics Communications,* **49**, 475-505 (1988)
30 A. Pak *et al., Review of Scientific Instruments*, **75**, 3747 (2004)

FIG. 1. Experimental pump-probe set up and targets configuration at GEKKO XII. The angular-resolved spectrometer was made by a defocused cylindrical Von Hamos geometry. For a better understanding of the geometry, the shielding of the spectrometer that surrounds the HOPG crystal and the Image Plate is not represented here.

FIG. 2. On the left: raw diffractograms collected in reflection by the defocused Von Hamos spectrometer on three different laser shots. The first order used for the crystal configuration introduced spherical aberrations, corrected in our analysis. On the right: angular profiles of the diffracted signal after this correction (color lines) and theoretical predictions at the pressure measured by the VISAR system (black dashed lines normalized in height at the experimental signal).

FIG. 3. On top: hydrodynamic simulation made with the pulse features of the GEKKO XII laser and an intensity of 5.10^{12} W/cm^2. The probe was sent 1.1 ns later than the pump laser generating the shock (here at 1.0 ns). The rectangular box in blue defines the spatial and temporal windows probed by the X-rays, taking into account the absorption on a round trip in CH and iron (bottom graph). The analysis took in consideration the whole thickness of the target. In this layout, a large part of the probed iron was still at ambient pressure and temperature. Integrating spatially and temporally the hydrodynamic conditions of the probed shocked iron gave an average pressure of 106 +/- 7 GPa. The uncertainty corresponds to the standard deviation of the reached pressures in the 20 µm 1.6 ns temporal and spatial windows investigated.